



Synergistic Effect of Surface Coating and Multi-additive-Based Electrolyte for Enhancing the Cycling Performance of LiMn_2O_4 Cathodes

Ngoc Thi Bao Nguyen¹ · Ni Truong Nhat Nguyen¹ · Hoang Van Nguyen^{2,3} · Nhan Thanh Tran² · Trung Thien Nguyen^{3,4} · Quan Dinh Nguyen^{3,5} · Quan Phung^{1,3} · Phung My Loan Le^{1,2,3}  · Duc Quang Truong⁶ · Man Van Tran^{1,2,3}

Received: 13 November 2022 / Accepted: 20 January 2023 / Published online: 24 February 2023
© The Minerals, Metals & Materials Society 2023

Abstract

Spinel LiMn_2O_4 (LMO) has been recognized as one of the most competitive cathode candidates for lithium-ion batteries, ascribed to the environmentally benign and abundant source. Nevertheless, LMO suffers from rapid capacity fading, preventing its wider application. To effectively overcome this issue, this work focused on the surface modification of pristine LMO powder with ZnO and Al_2O_3 thin layers by the precipitation method, which dramatically reduced dissolution loss of active Mn and the notorious cooperative Jahn–Teller distortion during the charge–discharge process. In addition, the use of multiple additives [fluoroethylene carbonate (FEC), succinonitrile (SN), and lithium bis(oxalato)borate (LiBOB)] in 1.5 M LiPF_6 EC:EMC:DMC (2:1:7, v/v/v) showed a collective impact on the enhanced long-cycling performance of the half-cell and full cell. It was revealed that ZnO -coated LMO (LMO@ZnO) and Al_2O_3 -coated LMO ($\text{LMO@Al}_2\text{O}_3$) powder exhibited good crystallinity and maintained a stable crystal structure during cycling compared with pristine LMO. In the multi-additive-based electrolytes, the graphite || LMO@ZnO full cell exhibited initial discharge capacity of 117.2 mAh/g, with 86.69% capacity retention after 100 cycles at C/3, while the full-cell graphite || LMO@ZnO performance exhibited slightly lower capacity retention of 80.79% after 100 cycles. These results were attributed to the formation of the cathode–electrolyte interface (CEI) and the solid electrolyte interphase (SEI) layers with low charge transfer resistance, leading to enhanced cycling performance and rate capability.

Keywords Al_2O_3 coating · electrolyte additive · LiMn_2O_4 · lithium-ion batteries · ZnO coating

Introduction

Since their commercialization in 1991, lithium-ion batteries (LIBs) have become an effective solution for powering electronic devices and have recently been considered as a green energy storage solution for renewable energy as well as for electric transportation.¹ In developing large-scale lithium-ion technology, spinel LiMn_2O_4 (LMO) has been regarded as one of the most prospective materials for the LIBs due to its advantages of easy to preparative, low cost, environmentally friendly nature, high working voltage (≥ 4 V), and high-rate capability.^{2,3} Nevertheless, the cycling instability of LMO is the main obstacle leading to its restricted application. Many reports have revealed that capacity loss had been ascribed to several factors, including (i) the dissolution of Mn^{3+} ion under an acidic environment due to the hydrolysis of LiPF_6 and (ii) the innate Jahn–Teller effect.⁴ To overcome

✉ Phung My Loan Le
lmlphung@hcmus.edu.vn

¹ Department of Physical Chemistry, Faculty of Chemistry, University of Science, Ho Chi Minh City, Vietnam

² Applied Physical Chemistry Laboratory (APCLAB), University of Science, Ho Chi Minh City, Vietnam

³ Vietnam National University, Ho Chi Minh City, Vietnam

⁴ Central Laboratory for Analysis, University of Science, Ho Chi Minh City, Vietnam

⁵ Biofuel and Biomass Research Laboratory, Faculty of Chemical Engineering, University of Technology (HCMUT), Ho Chi Minh City, Vietnam

⁶ Battery Cell Institute, Vinfast LLC, Cat Ba, Hai Phong City, Vietnam

its capacity fading, many methods have been considered. Among them, the substitution of heterogeneous atoms into the lattice with a small fraction of transition metals and the surface coating seem promising for practical application.⁵ As verified by many research investigations, the heterogeneous introduction of dopants into the cathode bulk structure suppressed the Jahn–Teller distortion. However, evidence on the efficiency of suppressing Jahn–Teller only by reducing the content of Mn^{3+} is still relatively limited.^{2,6–9} Therefore, the cathode surface coating has recently attracted attention because of its high efficiency in suppressing Mn dissolution and enhancing the SEI layer properties. Various oxides including MgO , TiO_2 , CeO_2 , ZnO , ZrO_2 , and Al_2O_3 have been proposed to effectively prevent capacity fading, indicating the effectiveness of surface modification on spinel $LiMn_2O_4$.^{10–14} For instance, Al_2O_3 has emerged as a solid protector due to its high-temperature stability and chemically inert characteristics in alkaline and acidic environments. It was reported that Al_2O_3 -coated LMO prepared by the sol–gel process could perform at elevated temperatures with a low capacity loss of about 10–15%.^{15,16} In addition, the coated layer properties impact not only Li-ion diffusion but also the Mn^{2+} dissolution effect on the cycling performance of LMO. To increase the diffusibility of the coating, Zhu et al. synthesized Al_2O_3 /PPy-coated LMO by the sol–gel method with a three-dimensional (3D) framework structure to increase the surface area and enhance the Li^+ ion conducting channels, and its electrochemical performance revealed high discharge capacity of 121.73 mAh/g at 1C along with capacity retention of 95.81% after 100 cycles.¹⁷ Meanwhile, Liu's research group coated the ZnO layer on LMO by co-precipitation, resulting in discharge capacity retention of 97% loss of only 3% after 60 cycles (121 mAh/g and 117 mAh/g).¹⁸ Shi and co-workers¹⁴ also synthesized porous $LiMn_2O_4$ by co-precipitation and then coated Al_2O_3 using the sol–gel method. The results indicated that the capacity retention was 98.6% and 91.2% at 25°C and 55°C after 100 cycles, respectively; at 10°C, the capacity remains stable at 94.4 mAh/g.

Apart from coating strategies, electrolytes also play an important role in stabilizing cell operation. Many studies have revealed that high-concentration electrolytes (HCE) can extend the cycle life and enhance the rate capacity of high-energy-density batteries due to the formation of robust SEI layer.^{19–22} However, HCE usually has high viscosity which impedes the battery's high-rate performance. In contrast, localized high-concentration electrolyte (LCHE) using a fluorinated diluent to decrease the viscosity and maintain the interfacial properties has attracted considerable attention in significantly. In addition, these electrolytes typically have high viscosity compared to conventional carbonate-based electrolytes. Besides, different additives have been additionally used in LCHE to stabilize the SEI layer for achieving

long-cycling performance, such as difluorobis(oxalato)phosphate (LiDFBOP), 4-chloromethyl-1,3,2-dioxathiolane2-oxide (CMDO), $LiPO_2F_2$, fluorosulfonyl isocyanate (FI), and fluoroethylene carbonate (FEC). Specifically, Taskovic et al. optimized the additive amount of vinylene carbonate and ethylene sulfate in 1.33 M $LiPF_6$ in EC:EMC:DMC (25:5:70, v/v/v) to prolong charge–discharge cycling for graphite|| $LiNi_{0.5}Mn_{0.3}Co_{0.2}O_2$.²³ Jianhui et al. discovered that replacing the dilute electrolyte with 5.5 M $LiN(SO_2F)_2$ (LiFSA)/dimethyl carbonate (DMC) electrolyte greatly inhibited the dissolution of transition metals of graphite|| $LiNi_{0.5}Mn_{1.5}O_4$, where a peculiar 3D connectivity of ionic species and solvent molecules coordinated with Li^+ form.^{24,25}

Herein, the long cycling performance of the graphite||LMO full cell can be achieved by employing the coating process and multi-additives supporting electrolytes to mitigate Mn dissolution and reinforce the SEI layer. The ZnO-coated LMO (LMO@ZnO) and Al_2O_3 -coated LMO (LMO@ Al_2O_3) samples were prepared by the coprecipitation method. The evaluation of electrochemical performance was conducted in different additives, including fluoroethylene carbonate (FEC), 0.5 wt.% succinonitrile (SN), and 1 wt.% lithium bis(oxalato)-borate (LiBOB) combined in the high-concentration electrolyte of 1.5 M $LiPF_6$ in EC: EMC: DMC (2:1:7, v/v/v).

Experimental

Preparing Al_2O_3 and ZnO-Coated LMO

The LMO (commercial powder, MTI Corp., USA) coating by oxide layer was conducted in an aqueous solution. Preparation of Al_2O_3 or ZnO-coated $LiMn_2O_4$ material includes: 5 mmol $LiMn_2O_4$ powder mixed with 0.5 mmol $Al(NO_3)_3 \cdot 6H_2O$ or 0.5 mmol $Zn(NO_3)_2 \cdot 10H_2O$ in 25 mL of distilled water. Then, the pH of the dispersed solution was adjusted to 8 by adding NH_3 25 wt.% solution to precipitate Al^{3+} and Zn^{2+} ions ultimately. The mixture was stirred for 4 h before filtering and drying at 80°C. Finally, the dried powder was heated at 350°C in the air for 3 h. The content of Al_2O_3 or ZnO coating is expected to be about 2–3 wt.%, which has less impact on the electronic conductivity of $LiMn_2O_4$ itself.^{25,26}

Electrolyte Preparation

Carbonate solvents including ethylene carbonate (EC), dimethyl carbonate (DMC), and ethyl methyl carbonate (EMC) of battery grade supplied from Sigma-Aldrich were dried with a molecular sieve prior to use. Lithium salts, including $LiPF_6$

(Solvionic, 99.99%) and LiBOB (Solvionic, 99.99%), were stored in a glove box. The solvent additives fluoroethylene carbonate (FEC, Sigma-Aldrich, 99.5%), succinonitrile (SN, Sigma-Aldrich, 99%), and ethylene sulfate (ESA, Aldrich, 99%) were alternatively mixed at different concentrations with carbonate solvents, as shown in Table I.

Material Characterization

The structure of the samples was characterized with x-ray diffraction (XRD, D8 Advance, Bruker) using a Cu-K α ($\lambda = 1.5418 \text{ \AA}$) radiation source in the range of $10^\circ \leq 2\theta \leq 70^\circ$. The morphology of the synthesized powder was observed by scanning electron microscopy (SEM, S4800, Shimadzu) coupled with energy-dispersive spectroscopy (EDS) for the elemental distribution and quantitative analysis.

Electrode Preparation and Cell Assembly

The cathode composition consists of the bare or coated LMO (MTI, 99.9%), conductive carbon C65 (Imerys), and PVDF (polyvinylidene fluoride) dissolved in 10 wt.% in *N*-methylpyrrolidone (NMP) in a weight ratio of 80:15:5. The cathode mixture was mixed in a THINKY mixer to obtain a homogeneous slurry, then cast on aluminum foil using the doctor blade technique. Then, the electrode film was dried in a vacuum chamber at 80°C for 12 h and punched into 13 mm-diameter ground shape (loading active mass $\sim 3 \text{ mg cm}^{-2}$).

The anode was made of commercial graphite (MTI Corp., 90 wt.%), C65 (Imerys, 5 wt.%), and the binder CMC/SBR (1:1 in weight, at 5 wt.%), which was dissolved in water at the concentration of 1.4 wt.% for CMC (Sigma-Aldrich, $M_w = 2,500,000$) and 25 wt.% for SBR (MTI Corp.), respectively. The mixture was thoroughly mixed to make a slurry and then cast on copper foil. The electrode film was then dried at 80°C in a vacuum for 12 h and punched into anode disks 13 mm in diameter (loading mass $\sim 1.5 \text{ mg/cm}^2$).

A CR2032 coin cell type was used for electrochemical characterization, and the cell assembly was conducted in an Ar-filled glove box (MBraun, Germany) with O₂/H₂O concentration below 1 ppm. The electrolytes were prepared

by dissolving lithium salt/additives into the mixture of solvents. The composition of the electrolytes used in this work is given in Table I. The half-cell consists of the as-prepared cathode as the working electrode, lithium foil with 14 mm diameter as the counter and reference electrodes, and PP (polypropylene) as the separator soaked in different electrolytes (see Table I). The lithium foil was replaced for the full-cell configuration by the as-prepared graphite anode. The anode and cathode capacity ratio (N/P ratio) for the full cell was roughly 1.2 as calculated from the reversible capacity of the electrodes. In the case of the prelithiation techniques applied, the anode electrode was in direct contact with lithium metal 15 min before the cell assembly. Li/Li symmetric cells were assembled using two Li metal foils as electrodes and PP soaked with 100 μL testing electrolyte as a separator. In linear sweep voltammetry (LSV) testing, Li metal served as both the reference and counter electrode.

The charge/discharge performance and rate capability tests were conducted on a LAND battery tester (Wuhan LAND Electronic Co., China) in the potential range of 3.0–4.5 V versus Li⁺/Li for the half-cell and 3.0–4.3 V for the full cell at C/3. LSV was conducted at a scan rate from 0.1 mV/s open-circuit potential to 6.5 V. Li/Li symmetric cells were cycled with a capacity of 1 mAh/cm² at a charge/discharge rate of 0.5 mA/cm². Electrochemical impedance spectroscopy (EIS) was performed on a VSP-3 potentiostat (BioLogic, France) in a frequency range of 1 MHz to 0.1 Hz with the amplitude of the potential signal of 10 mV.

Results and Discussion

Characterization and Morphology of the Coated LMO Samples

Figure 1a shows the XRD patterns for pristine LMO, LMO@Al₂O₃, and LMO@ZnO. As can be seen, all the diffraction peaks are indexed with the spinel structure of LiMn₂O₄ (JCPDS card No. 35-0782, space group of Fd-3 m). These peaks, corresponding to crystal planes, are labeled on the patterns. The XRD patterns are almost the same in the coated samples, with no impurities detected. The coating is a relatively thin layer covering the LMO surface and has a low concentration of oxide, which is lower

Table I The composition of the electrolytes

ID	Salt	Solvents	Additives
Baseline	1.5 M LiPF ₆	EC: EMC: DMC (2:1:7, v/v/v)	None
E1	1.5 M LiPF ₆	EC: EMC: DMC (2:1:7, v/v/v)	5 wt.% FEC: 0.5 wt.% SN: 1 wt.% LiBOB
E2	1.5 M LiPF ₆	EC: EMC: DMC (2:1:7, v/v/v)	5 wt.% FEC: 0.5 wt.% SN: 1 wt.% LiBOB: 1 wt.% ESA
E3	1.5 M LiPF ₆	EC: EMC: DMC (2:1:7, v/v/v)	7 wt.% FEC: 0.5 wt.% SN: 1 wt.% LiBOB

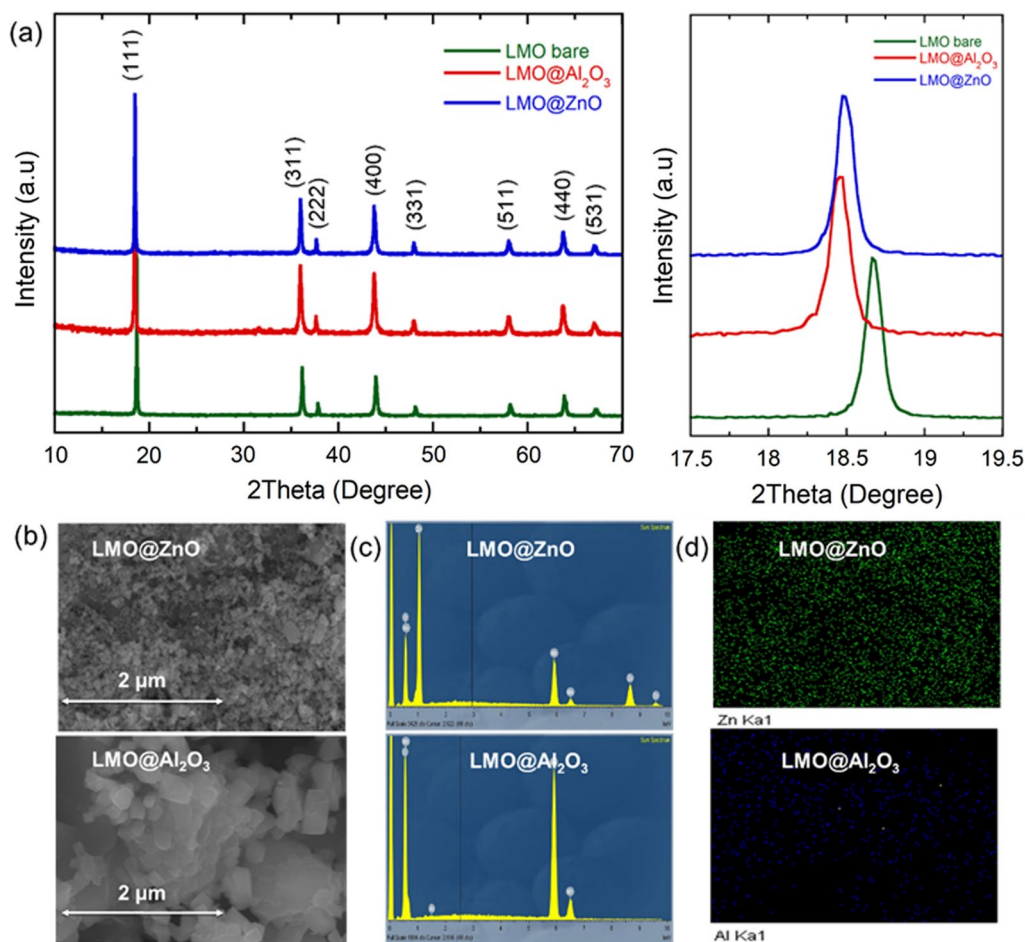


Fig. 1 (a) X-ray diffraction patterns of pristine LMO and coated LMO, (b) SEM images, (c) EDX spectrum oxide-coated LMO, (d) Element distribution in the selected area.

Table II Lattice parameters of the bare LMO and the coated LMO with 5 wt.% transition metal oxide

Sample ID	Lattice parameter (Å)	Volume (Å ³)
Bare LiMn ₂ O ₄	8.245	560.50
LiMn ₂ O ₄ @Al ₂ O ₃	8.261	563.72
LiMn ₂ O ₄ @ZnO	8.254	562.36

than the detection limit by XRD.^{24–27} Compared with the bare LMO, the coated samples displayed a broadening of peaks, indicating the surface modification of LMO by the coated layers (Fig. 1b). Table II displays the change in the lattice parameter and volume with the coating of Al₂O₃ and ZnO calculated using Celref V3 software. As can be seen, the crystalline lattice of LiMn₂O₄ is enlarged after coating, which reflects a small portion of cations diffused from the oxide into the LMO structure under synthesis conditions. It is noticeable that the lattice constant and volume increased slightly for both LiMn₂O₄@Al₂O₃ and LiMn₂O₄@ZnO.

Zhou et al. reported similar results when coating LMO with different Al₂O₃ amounts. However, due to the high temperature used for coating, the diffraction pattern (440) moved leftward compared to pristine LMO at the same amount of Al₂O₃ surface-modified spinel LMO, indicating the smaller lattice parameter of the pristine sample.²⁵ EDS and SEM analysis were further employed to study the morphology and the composition of the LiMn₂O₄ surface-treated (Fig. 1c, d). SEM reveals that the LMO@ZnO consists of small ZnO particles, while large Al₂O₃ particles are observed for LMO@Al₂O₃. EDS spectra results eventually confirm the appearance of ZnO and Al₂O₃ and the homogenous contribution of the elements on the surface of the coated LMO. In addition, the low peak intensity of Al₂O₃ is similarly reported for Al₂O₃@LiMn₂O₄ at only ~2 wt.% of Al₂O₃ while the intense peak of Al₂O₃ was observed for ZnO@LiMn₂O₄ coated with 3 wt.%

Figure 2 shows the Raman spectra of bare and coated LMO in the region of 100–800 cm⁻¹. As can be seen, the spectra presented similar features including a strong band

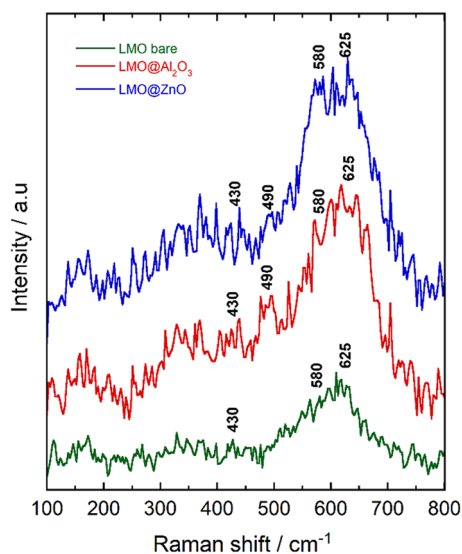


Fig. 2 (a) Raman spectra of the bare and coated LMO samples.

around 625 cm^{-1} and a group of bands in the $300\text{--}500\text{ cm}^{-1}$ region.^{22,23} For cubic spinel LiMn_2O_4 and other manganese oxides, the strong bands in the spectral region $550\text{--}700\text{ cm}^{-1}$ are characteristic of Mn–O vibrations and closely related to the oxidation state of manganese.^{22,23} Meanwhile, the weaker bands in the $300\text{--}500\text{ cm}^{-1}$ region are featured of Li–O vibration. The shoulder peak at around 580 cm^{-1} in the spectra may originate from the vibration of $\text{Mn}^{\text{IV}}\text{--O}$ bonding²² because of the 2 oxidation state of the manganese ions in the spinel structure. For the coated LMO samples, the presence of other metals besides manganese was attributed to the Raman enhancement efficiency, thus improving the intensity. Typically, Al_2O_3 and ZnO possess the highest Raman reflective bands at 416 cm^{-1} and 580 cm^{-1} , respectively,^{24,25} which are almost the same and are superposed to the corresponding bands of the spinel structure at 430 cm^{-1} and 580 cm^{-1} . Therefore, the improvement in Raman band intensity at around 430 cm^{-1} and 580 cm^{-1} in the $\text{LMO@Al}_2\text{O}_3$ and LMO@ZnO spectra revealed the presence of Al_2O_3 and ZnO coating on the surface of LMO particles.

Effect of the Coating Layer on the Half-Cell Performance

The rate capability test of the cathodes is shown in Fig. S1. The LMO@ZnO exhibited superior discharge capacity relative to other cathodes, in both low-rate and high-rate capacity. Specifically, at current density of $C/5$, LMO@ZnO showed significantly higher discharge capacity of 110.3 mAh/g compared with 100.6 mAh/g for bare LMO. Moreover, bare LMO and $\text{LMO@Al}_2\text{O}_3$ were unable to

operate at current density of $4C$, while LMO@ZnO exhibited discharge capacity of 51.5 mAh/g .

The voltage profiles of the materials shown in Fig. 2a display relatively high distortion due to the irreversibility of the electrolyte reaction at the electrode surface on charge. Figure 2b compares the discharge capacity versus cycle number to show the cycling performance of bare LMO and oxide-coated LMO at rate $C/3$ during 100 cycles. The oxide coating helped to improve the long-cycling performance of LMO significantly. By coating the oxide layer, the initial discharge capacity of $\text{LMO@Al}_2\text{O}_3$ (106.2 mAh/g) is slightly lower than that of bare LMO (111.6 mAh/g); however, its capacity retention of $\text{LMO@Al}_2\text{O}_3$ is much higher compared to the pristine one (95.86% versus 80.56%) after 100 cycles. Therefore, the Al_2O_3 coating layer partially protects the active material LMO from direct reaction with the electrolyte and mitigates the Mn dissolution in the electrolyte during cycling. Furthermore, it was also reported that the possible formation of second phase $\text{LiAl}_y\text{Mn}_{2-y}\text{O}_4$ on the LiMn_2O_4 surface, with a high amount of Al_2O_3 coating, strengthens the spinel structure and mitigates the loss of manganese.¹⁰ Regarding the LMO@ZnO sample, the specific discharge capacity is slightly higher than that of the bare LMO (105.5 mAh/g), with the same capacity retention as $\text{LMO@Al}_2\text{O}_3$. In Fig. 2c, the coulombic efficiency of the bare LMO and coated LMO electrodes are largely the same ($\sim 97\%$) after a few cycles. Although the effectiveness of the coating process led to the enhancement of the initial coulombic efficiency (from $\sim 80\%$ to $> 85\%$), it was observed that the high interfacial resistance still originated from the surface passivation induced by the side reaction with the baseline electrolyte.²¹ This highlights the role of additive-based electrolytes in reducing unexpected reaction and stabilizing the electrode–electrolyte interface during cycling.

In Fig. 3d, the Nyquist plot indicates the impedance of half-cells, which generally displays a similar semicircle feature at high frequency and a long linear diffusion line at a lower frequency. The lower diameter of the semicircle of the LMO-coated electrode reveals that the coating layer improved the charge transfer reaction step at the electrolyte interface associated with the cycling performance improvement.

Role of the Additives in Stabilizing the Cycling Performance

Figure 4a shows the effect of additives on the electrochemical window of the electrolytes. The baseline electrolyte is oxidized at about 5.0 V versus Li^+/Li . However, by adding the additives (FEC, SN, LiBOB, ESA), the electrolyte oxidation starts at the higher potential range of $5.5\text{--}6.0\text{ V}$. To further explore the beneficial effect of the additives, Li ||

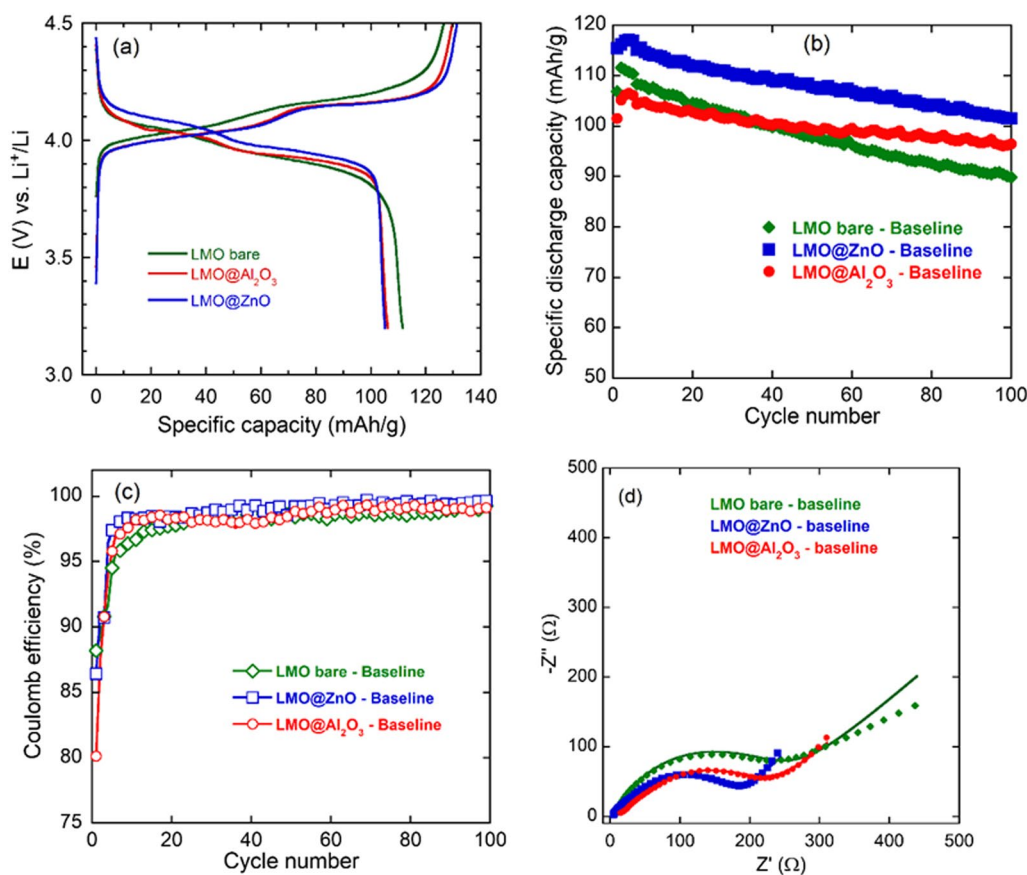


Fig. 3 (a) Voltage profiles, (b–c) cycling performance, (d) Nyquist plot of bare LMO half-cell, LMO@ZnO, LMO@Al₂O₃ (experimental: dots, fitting curve: solid line).

Li symmetric cell using these three electrolytes was tested at current density of 0.5 mA/cm² with capacity of 1 mAh/cm². As shown in Fig. 4b, the E2 and E3 electrolytes with FEC and SN addition exhibited a negligible overpotential in 450 h (E1) and 500 h (E3 with higher FEC concentration), indicating a stable interface with the Li metal anode in these electrolytes. Indeed, the higher amount of FEC in the electrolyte offers the lowest overpotential in the symmetrical cell due to the enhancement of the fluorine-rich SEI layer. Consequently, the robust SEI layer built up during cycling with the addition of the additives could limit the further decomposition of the electrolytes and the passivation of the electrode surface by the side products.

As seen in Fig. 5a and Table III, it can be confirmed that E2 preserves better Li-ion diffusion in the bulk material due to the smallest semicircle radius for the Li || LMO@ZnO and Li || LMO@Al₂O₃ half-cells. Furthermore, the Li || LMO@Al₂O₃ half-cell exhibited the lowest charge transfer resistance and SEI layer resistance, indicating that the side reaction between electrode–electrolyte or Mn dissolution was successfully minimized.

Despite the lowest discharge capacity, the coulombic efficiency (~99.5% after a few cycles) and capacity retention of the Li || LMO@ZnO cell in E2-based electrolyte are the highest among the electrolytes, at about 80% after 100 cycles at C/3 (Fig. 6c). The presence of ESA in the E2 electrolyte decreased the ionic conductivity, leading to a decrease in discharge capacity. This was attributed to the reduced decomposition of ESA, leading to the formation of large molecules dissolved in solvent, which eventually enhanced the viscosity and reduced the ionic conductivity of the electrolyte [29]. The comparison of E2 and E3 with different FEC concentrations shows that 5 wt.% FEC achieved a better effect than 7 wt.% FEC in LMO@Al₂O₃- or LMO@ZnO-coated cathodes (Fig. 5a, b, c and d). Higher FEC additive content without ESA addition induced fast capacity decay and unstable coulombic efficiency in the case of LMO@Al₂O₃. Regarding the Li||LMO@ZnO half-cell, the E1 electrolyte with 5 wt.% FEC showed the best performance, with discharge capacity of 109.0 mAh/g and remained at 86.49% after 100 cycles.

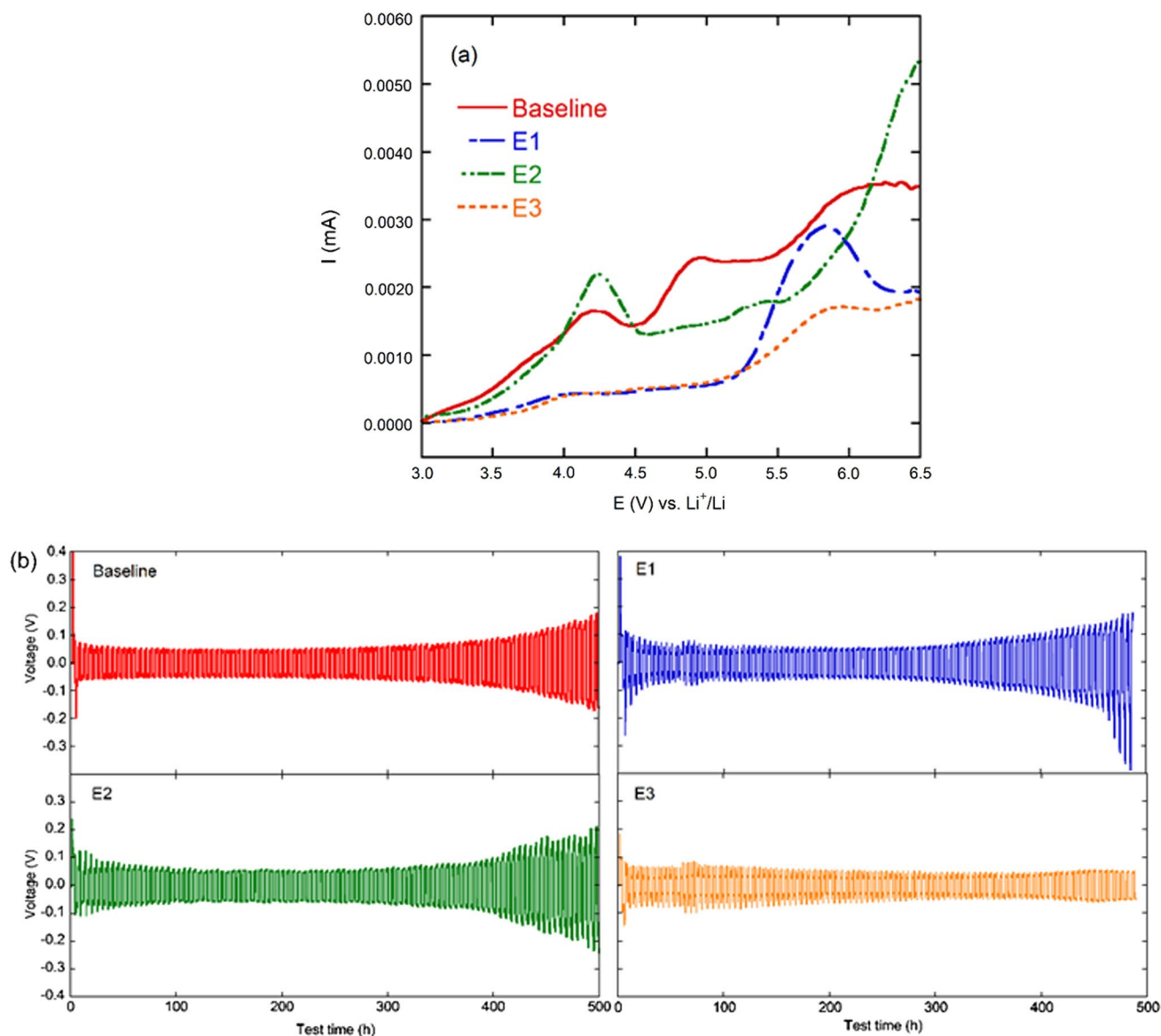


Fig. 4 (a) LSV curve of different electrolytes in the range 3.0–6.5 V, (b) cycling performance of Li–Li symmetric cells at a capacity of 1 mAh/cm² and current density of 0.5 mA/cm².

In the full-cell configuration, the LMO cathodes coated with ZnO and Al₂O₃ are coupled with graphite and cycled in different electrolytes, as shown in Fig. 7. Typically, a prelithiation process is used to improve the coulombic efficiency of anodes by the formation of an SEI layer prior to cycling.²⁶ In this way, the lithium lost during electrolyte decomposition to form the SEI can be compensated, and the anode side is much more protected. Moreover, the formation of SEI on the graphite anode, which plays a vital role in the desolvation of lithium ions, is much more sensitive to the electrolyte

composition and additives. As a result, the quantity and nature of the additives can alter the thickness, composition, and, as a result, the SEI quality.²⁷ Briefly, prelithiation is useful in the case of an LMO high-voltage cathode coupled with a graphite anode owing to the compensation of irreversible capacity lost for electrolyte decomposition and the formation of the SEI layer (Fig. 7a). The performance of the cells using a prelithiated anode is evaluated in different electrolyte compositions shown in Fig. 7b, c and d. E1 with lower FEC concentration exhibited a higher discharge

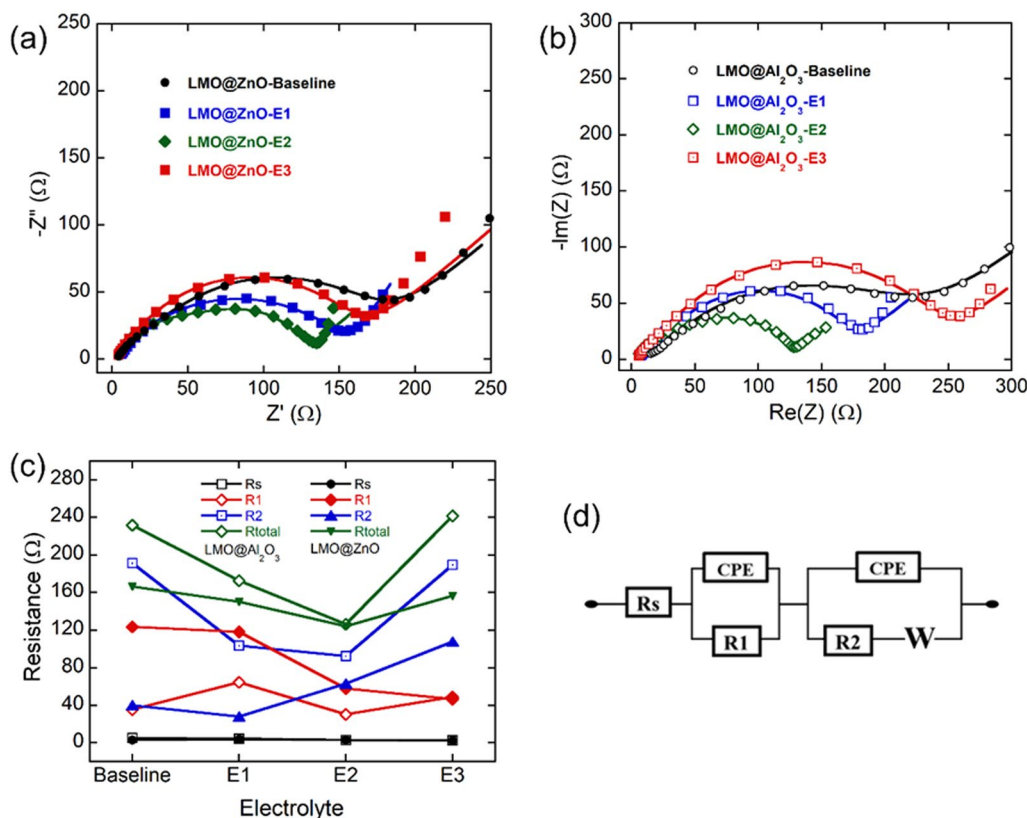


Fig. 5 Nyquist plot of half-cells (a) Li || LMO@Al₂O₃ and (b) Li || LMO@ZnO in different testing electrolytes, (c) resistance values fitted using the equivalent circuit and (d) physical equivalent circuit.

Table III Different resistance values fitted by the equivalent circuit from Fig. 3b

	R _s	R1 (Charge transfer)	R2 (SEI layer)	R _{total}
Bare LMO				
	3.517	0.46	211.0	214.9
LMO@Al₂O₃				
Baseline	5.237	35.36	191.20	231.80
E1	4.606	64.61	103.40	172.62
E2	3.281	30.45	92.51	126.24
E3	2.861	49.05	189.60	241.51
LMO@ZnO				
Baseline	3.016	123.50	39.98	166.50
E1	3.788	118.30	28.01	150.10
E2	3.112	63.01	57.97	124.09
E3	3.247	73.55	49.34	126.14

capacity of 105 mAh/g. Although coulombic efficiency is nearly the same (~90%, respectively) when cycling the

cells in three electrolytes (Fig. 7d), FEC offers better capacity retention due to the formation of thin, flexible Li-ion-conducting surface films with excellent protective properties. For the graphite || LMO@ZnO full cell, the capacity retention in the E2 and E3 electrolytes is almost the same, but the E1 electrolyte exhibits stable, moderate discharge capacity without fluctuation, which is also coherent with the performance of the Li || LMO@ZnO half-cell (Fig. 6c and d). Regarding the graphite || LMO@Al₂O₃ full cell, the E2 electrolyte exhibited the lowest discharge capacity, as expected, compared to the E1 and E3 electrolytes. This result was attributed to the low ionic conductivity of the E2 electrolyte and is also compatible with the performance of the Li || LMO@Al₂O₃ half-cell (Fig. 5a and b).

The performance in different rates (C/5, C/2, C, 2C, 3C, 4C, C/5) in the graphite || coated LMO full cell was also evaluated (Fig. 7e–f). The rate performance of the full cell is dependent on the difficulty of Li-ion diffusion in the cathode and anode material structure and bulk electrolyte with separator.¹² As expected, the full cells operated in the E2 electrolyte exhibited better rate capability for Al₂O₃-coated and

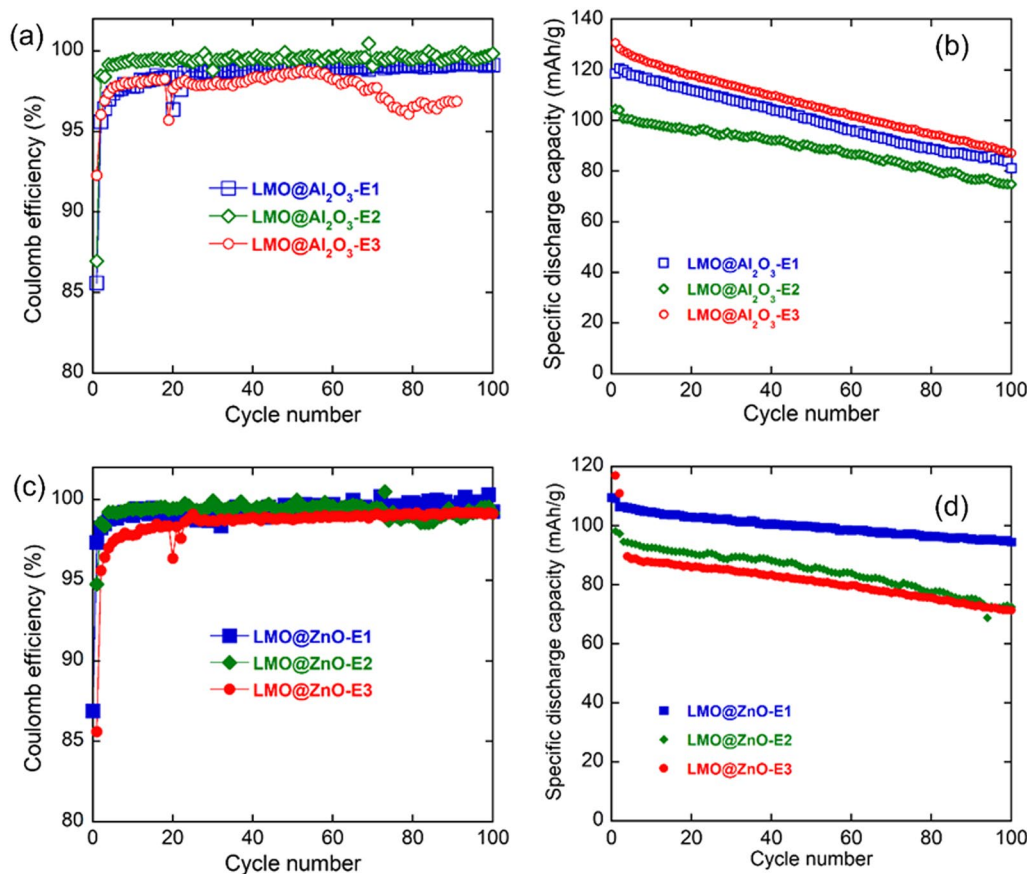


Fig. 6 Discharge capacity and coulombic efficiency versus cycle number: (a, b) half-cell Li || LMO@Al₂O₃ and (c–d) half-cell Li || LMO@ZnO.

ZnO-coated LMO than other cells due to its lowest charge transfer and SEI resistance (Table III). A suitable concentration FEC (E2 with 5 wt.% FEC in this work) can improve the cell performance at high rates because the SEI on graphite formed by FEC reduction is less resistive than conventional alkyl carbonates-based SEI, allowing for faster intercalation/deintercalation.^{26,27} The oxide coating layer properties also have a significant impact on the performance of the cells at high rates. Al₂O₃ has been reported to limit Li⁺ diffusion due to its dense layer structure.¹¹

Meanwhile, ZnO, with an amorphous structure and higher porous density, is suitable for electrolyte filling the void in the electrode and decreasing the Li-ion diffusion path. Hence, a full cell with LiMn₂O₄@ZnO cathode exhibited better rate performance, as shown in Fig. 5f. Furthermore, after cycling at a high rate of 4C and switching back to a low rate (C/5), the specific capacity of full cells is almost unchanged, confirming an excellent stable spinel structure.

Conclusion

In summary, this study evaluated the synergistic effect of coating an LMO cathode with ZnO and Al₂O₃ and multiple additives together with high-concentration electrolyte 1.5 M LiPF₆, EC:EMC:DMC (2:1:7, v/v/v) for the half-cell and full cell with anode graphite. In the half-cell, the Li||LMO@ZnO cell with 5 wt.% FEC/0.5 wt.% SN/1 wt.% LiBOB electrolyte exhibited the best performance, with specific capacity of 117.2 mAh/g and 86.69% capacity retention after 100 cycles at C/3. Additionally, the graphite || LMO-coated (ZnO and Al₂O₃ similar) full cell showed good retention of discharge capacity (80.8% of initial capacity) after 100 cycles at C/3. Therefore, the combination of cathode interphase modification by coating and the use of different additives boosts the cell's long cycling performance in both the half-cell and full cell with graphite. Further work will be essential to enhancing the rate capability of the full cell.

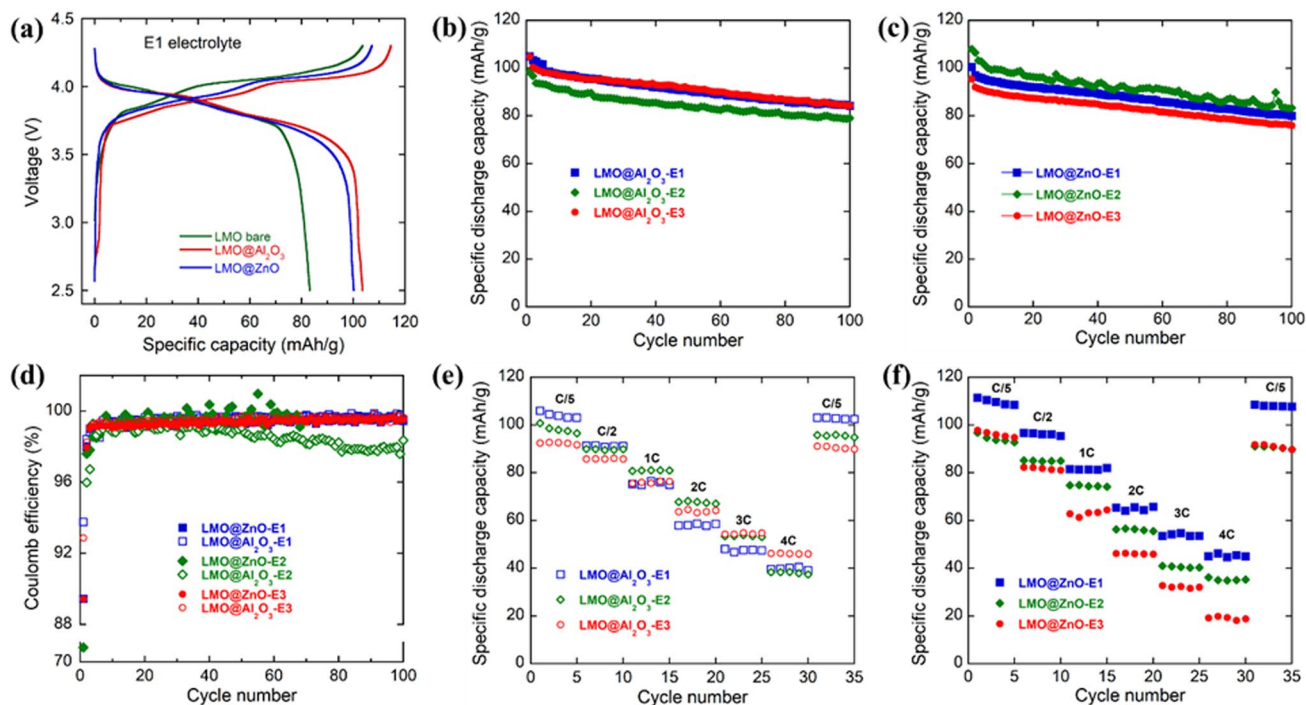


Fig. 7 Cycling performance of graphite || LMO full cells: (a) voltage profiles of the full cell with bare LMO, LMO@Al₂O₃, and LMO@ZnO in E1 electrolyte, discharge capacity versus cycle number of (b)

LMO@Al₂O₃ and (c) LMO@ZnO in different electrolytes, (d) coulombic efficiency versus cycle number, rate capability of the full cell with (e) LMO@Al₂O₃ and (f) LMO@ZnO.

Supplementary Information The online version contains supplementary material available at <https://doi.org/10.1007/s11664-023-10273-5>.

Acknowledgments This work was funded by Vingroup Joint Stock Company and supported by the Vingroup Innovation Foundation (VINIF) in project code VINIF.2020.NCUD.DA039.

Competing interests The authors declare that they have no conflict of interest.

References

1. X. Shen et al., Advanced electrode materials in lithium batteries: retrospect and prospect. *Energy Mater. Adv.* 2021, 1 (2021).
2. C. Jiang, Z. Tang, S. Wang, and Z. Zhang, A truncated octahedral spinel LiMn₂O₄ as high-performance cathode material for ultrafast and long-life lithium-ion batteries. *J. Power Sources* 357, 144 (2017).
3. J. Abou-Rjeily, I. Bezza, N.A. Laziz, C. Autret-Lambert, M.T. Sougrati, and F. Ghamouss, High-rate cyclability and stability of LiMn₂O₄ cathode materials for lithium-ion batteries from low-cost natural B-MnO₂. *Energy Storage Mater.* 26, 423 (2020).
4. C. Li, H.P. Zhang, L.J. Fu, H. Liu, Y.P. Wu, E. Rahm, R. Holze, and H.Q. Wu, Cathode materials modified by surface coating for lithium ion batteries. *Electrochim. Acta* 51, 3872 (2006).
5. M.S. Al Ja'farawy, D.N. Hikmah, U. Riyadi, A. Purwanto, and H. Widiyandari, A review: the development of SiO₂/C anode materials for lithium-ion batteries. *J. Electron. Mater.* 50, 6667 (2021).
6. Z. Wang, J. Du, Z. Li, and Z. Wu, Sol-gel synthesis of co-doped LiMn₂O₄ with improved high-rate properties for high-temperature lithium batteries. *Ceram. Int.* 40, 3527 (2014).
7. M.A. Kebede, N. Kunjuzwa, C.J. Jafta, M.K. Mathe, and K.I. Ozoemena, Solution-combustion synthesized nickel-substituted spinel cathode materials (LiNi_xMn_{2-x}O₄; 0 ≤ x ≤ 0.2) for lithium ion battery: enhancing energy storage, capacity retention, and lithium ion transport. *Electrochim. Acta* 128, 172 (2014).
8. H. Zhao, X. Bai, J. Wang, D. Li, B. Li, Y. Wang, L. Dong, B. Liu, and S. Komarneni, Enhanced cycling stability through erbium doping of LiMn₂O₄ cathode material synthesized by sol-gel technique. *Materials* 11, 1558 (2018).
9. M. Madhu, A. Venkateswara Rao, and S. Mutyala, La and Ni Co-doping effect in LiMn₂O₄ on structural and electrochemical properties for lithium-ion batteries. *J. Electron. Mater.* 50, 5141 (2021).
10. National and Local Joint Engineering Laboratory for Lithium-ion Batteries and Materials Preparation Technology, Key Laboratory of Advanced Battery Materials of Yunnan Province, Faculty of Materials Science and Engineering, Kunming University of Science and Technology, Kunming 650093, China and Y. Zhang, Spinel LiMn₂O₄ with two-step nano-Al₂O₃ coating as high performance positive materials. *Int. J. Electrochem. Sci.* 6853 (2017).
11. H. Cao, B. Xia, Y. Zhang, and N. Xu, LiAlO-Coated LiCoO as cathode material for lithium ion batteries. *Solid State Ion.* 176, 911 (2005).
12. L. Zhu, Y. Zhang, X. Zhao, Y. Jiao, Z. Zhao, Y. Wang, and N. Yang, Polypyrrole/Al₂O₃/LiMn₂O₄ cathode for enhanced storage of Li ions. *Electrochem. Commun.* 124, 106951 (2021).

13. H. Liu, C. Cheng, and K. Zhang, The effect of ZnO coating on LiMn_2O_4 cycle life in high temperature for lithium secondary batteries. *Mater. Chem. Phys.* 101, 276 (2007).
14. C. Shi, P. Zhang, L. Chen, P. Yang, and J. Zhao, Effect of a thin ceramic-coating layer on thermal and electrochemical properties of polyethylene separator for lithium-ion batteries. *J. Power Sources* 270, 547 (2014).
15. X. Cao, H. Jia, W. Xu, and J.-G. Zhang, Review—Localized high-concentration electrolytes for lithium batteries. *J. Electrochem. Soc.* 168, 010522 (2021).
16. S. Perez Beltran, X. Cao, J.-G. Zhang, and P.B. Balbuena, Localized high concentration electrolytes for high voltage lithium-metal batteries: correlation between the electrolyte composition and its reductive/oxidative stability. *Chem. Mater.* 32, 5973 (2020).
17. G. Jiang, F. Li, H. Wang, M. Wu, S. Qi, X. Liu, S. Yang, and J. Ma, 15- Perspective on high-concentration electrolytes for lithium metal batteries. *Small Struct.* 2, 2000122 (2021).
18. T. Taskovic, L.M. Thompson, A. Eldesoky, M.D. Lumsden, and J.R. Dahn, Optimizing electrolyte additive loadings in NMC532/graphite cells: vinylene carbonate and ethylene sulfate. *J. Electrochem. Soc.* 168, 010514 (2021).
19. J. Wang, Y. Yamada, K. Sodeyama, C.H. Chiang, Y. Tateyama, and A. Yamada, Superconcentrated electrolytes for a high-voltage lithium-ion battery. *Nat. Commun.* 7, 12032 (2016).
20. H.-M. Zhou, Y.-H. Zhu, J. Li, W.-J. Sun, and Z.-Z. Liu, Electrochemical performance of Al_2O_3 pre-coated spinel LiMn_2O_4 . *Rare Met.* 38, 128 (2019).
21. C. Zhan, T. Wu, J. Lu, and K. Amine, Dissolution, migration, and deposition of transition metal ions in Li-ion batteries exemplified by Mn-based cathodes—a critical review. *Energy Environ. Sci.* 11, 243 (2018).
22. C.V. Ramana, M. Massot, and C.M. Julien, XPS and Raman spectroscopic characterization of LiMn_2O_4 Spinel. *Surf. Interface Anal.* 37, 412 (2005).
23. C.M. Julien, M. Massot, and C. Poinignon, Lattice vibrations of manganese oxides. *Spectrochim. Acta A Mol. Biomol. Spectrosc.* 60, 689 (2004).
24. S. Vural and Ö. Sari, Synthesis and characterization of SDS assistant α -alumina structures and investigation of the effect of the calcination time on the morphology. *Colloid Polym. Sci.* 297, 107 (2019).
25. M. Wang, F. Ren, J. Zhou, G. Cai, L. Cai, Y. Hu, D. Wang, Y. Liu, L. Guo, and S. Shen, N doping to ZnO nanorods for photoelectrochemical water splitting under visible light: engineered impurity distribution and terraced band structure. *Sci. Rep.* 5, 12925 (2015).
26. H. Shin, J. Park, A.M. Sastry, and W. Lu, Effects of fluoroethylene carbonate (FEC) on anode and cathode interfaces at elevated temperatures. *J. Electrochem. Soc.* 162, A1683 (2015).
27. B. Flamme, D.J. Yeadon, S. Phadke, and M. Anouti, Effect of fluorinated additives or co-solvent on performances of graphite// LiMn_2O_4 cells cycled at high potential. *J. Energy Chem.* 52, 332 (2021).

Publisher's Note Springer Nature remains neutral with regard to jurisdictional claims in published maps and institutional affiliations.

Springer Nature or its licensor (e.g. a society or other partner) holds exclusive rights to this article under a publishing agreement with the author(s) or other rightsholder(s); author self-archiving of the accepted manuscript version of this article is solely governed by the terms of such publishing agreement and applicable law.